

Dalitz analysis of the three-body charmless decay $B^0 \rightarrow K_S^0 \pi^+ \pi^-$

K. Abe,⁹ K. Abe,⁴⁷ I. Adachi,⁹ H. Aihara,⁴⁹ K. Aoki,²³ K. Arinstein,² Y. Asano,⁵⁴
 T. Aso,⁵³ V. Aulchenko,² T. Aushev,¹³ T. Aziz,⁴⁵ S. Bahinipati,⁵ A. M. Bakich,⁴⁴
 V. Balagura,¹³ Y. Ban,³⁶ S. Banerjee,⁴⁵ E. Barberio,²² M. Barbero,⁸ A. Bay,¹⁹ I. Bedny,²
 U. Bitenc,¹⁴ I. Bizjak,¹⁴ S. Blyth,²⁵ A. Bondar,² A. Bozek,²⁹ M. Bračko,^{9,21,14}
 J. Brodzicka,²⁹ T. E. Browder,⁸ M.-C. Chang,⁴⁸ P. Chang,²⁸ Y. Chao,²⁸ A. Chen,²⁵
 K.-F. Chen,²⁸ W. T. Chen,²⁵ B. G. Cheon,⁴ C.-C. Chiang,²⁸ R. Chistov,¹³ S.-K. Choi,⁷
 Y. Choi,⁴³ Y. K. Choi,⁴³ A. Chuvikov,³⁷ S. Cole,⁴⁴ J. Dalseno,²² M. Danilov,¹³ M. Dash,⁵⁶
 L. Y. Dong,¹¹ R. Dowd,²² J. Dragic,⁹ A. Drutskoy,⁵ S. Eidelman,² Y. Enari,²³ D. Epifanov,²
 F. Fang,⁸ S. Fratina,¹⁴ H. Fujii,⁹ N. Gabyshev,² A. Garmash,³⁷ T. Gershon,⁹ A. Go,²⁵
 G. Gokhroo,⁴⁵ P. Goldenzweig,⁵ B. Golob,^{20,14} A. Gorišek,¹⁴ M. Grosse Perdekamp,³⁸
 H. Guler,⁸ R. Guo,²⁶ J. Haba,⁹ K. Hara,⁹ T. Hara,³⁴ Y. Hasegawa,⁴² N. C. Hastings,⁴⁹
 K. Hasuko,³⁸ K. Hayasaka,²³ H. Hayashii,²⁴ M. Hazumi,⁹ T. Higuchi,⁹ L. Hinz,¹⁹ T. Hojo,³⁴
 T. Hokuue,²³ Y. Hoshi,⁴⁷ K. Hoshina,⁵² S. Hou,²⁵ W.-S. Hou,²⁸ Y. B. Hsiung,²⁸
 Y. Igarashi,⁹ T. Iijima,²³ K. Ikado,²³ A. Imoto,²⁴ K. Inami,²³ A. Ishikawa,⁹ H. Ishino,⁵⁰
 K. Itoh,⁴⁹ R. Itoh,⁹ M. Iwasaki,⁴⁹ Y. Iwasaki,⁹ C. Jacoby,¹⁹ C.-M. Jen,²⁸ R. Kagan,¹³
 H. Kakuno,⁴⁹ J. H. Kang,⁵⁷ J. S. Kang,¹⁶ P. Kapusta,²⁹ S. U. Kataoka,²⁴ N. Katayama,⁹
 H. Kawai,³ N. Kawamura,¹ T. Kawasaki,³¹ S. Kazi,⁵ N. Kent,⁸ H. R. Khan,⁵⁰
 A. Kibayashi,⁵⁰ H. Kichimi,⁹ H. J. Kim,¹⁸ H. O. Kim,⁴³ J. H. Kim,⁴³ S. K. Kim,⁴¹
 S. M. Kim,⁴³ T. H. Kim,⁵⁷ K. Kinoshita,⁵ N. Kishimoto,²³ S. Korpar,^{21,14} Y. Kozakai,²³
 P. Križan,^{20,14} P. Krokovny,⁹ T. Kubota,²³ R. Kulasiri,⁵ C. C. Kuo,²⁵ H. Kurashiro,⁵⁰
 E. Kurihara,³ A. Kusaka,⁴⁹ A. Kuzmin,² Y.-J. Kwon,⁵⁷ J. S. Lange,⁶ G. Leder,¹²
 S. E. Lee,⁴¹ Y.-J. Lee,²⁸ T. Lesiak,²⁹ J. Li,⁴⁰ A. Limosani,⁹ S.-W. Lin,²⁸ D. Liventsev,¹³
 J. MacNaughton,¹² G. Majumder,⁴⁵ F. Mandl,¹² D. Marlow,³⁷ H. Matsumoto,³¹
 T. Matsumoto,⁵¹ A. Matyja,²⁹ Y. Mikami,⁴⁸ W. Mitaroff,¹² K. Miyabayashi,²⁴ H. Miyake,³⁴
 H. Miyata,³¹ Y. Miyazaki,²³ R. Mizuk,¹³ D. Mohapatra,⁵⁶ G. R. Moloney,²² T. Mori,⁵⁰
 A. Murakami,³⁹ T. Nagamine,⁴⁸ Y. Nagasaka,¹⁰ T. Nakagawa,⁵¹ I. Nakamura,⁹
 E. Nakano,³³ M. Nakao,⁹ H. Nakazawa,⁹ Z. Natkaniec,²⁹ K. Neichi,⁴⁷ S. Nishida,⁹
 O. Nitoh,⁵² S. Noguchi,²⁴ T. Nozaki,⁹ A. Ogawa,³⁸ S. Ogawa,⁴⁶ T. Ohshima,²³ T. Okabe,²³
 S. Okuno,¹⁵ S. L. Olsen,⁸ Y. Onuki,³¹ W. Ostrowicz,²⁹ H. Ozaki,⁹ P. Pakhlov,¹³ H. Palka,²⁹
 C. W. Park,⁴³ H. Park,¹⁸ K. S. Park,⁴³ N. Parslow,⁴⁴ L. S. Peak,⁴⁴ M. Pernicka,¹²
 R. Pestotnik,¹⁴ M. Peters,⁸ L. E. Piilonen,⁵⁶ A. Poluektov,² F. J. Ronga,⁹ N. Root,²
 M. Rozanska,²⁹ H. Sahoo,⁸ M. Saigo,⁴⁸ S. Saitoh,⁹ Y. Sakai,⁹ H. Sakamoto,¹⁷
 H. Sakaue,³³ T. R. Sarangi,⁹ M. Satapathy,⁵⁵ N. Sato,²³ N. Satoyama,⁴² T. Schietinger,¹⁹
 O. Schneider,¹⁹ P. Schönmeier,⁴⁸ J. Schümann,²⁸ C. Schwanda,¹² A. J. Schwartz,⁵
 T. Seki,⁵¹ K. Senyo,²³ R. Seuster,⁸ M. E. Sevier,²² T. Shibata,³¹ H. Shibuya,⁴⁶
 J.-G. Shiu,²⁸ B. Shwartz,² V. Sidorov,² J. B. Singh,³⁵ A. Somov,⁵ N. Soni,³⁵ R. Stamen,⁹
 S. Stanič,³² M. Starič,¹⁴ A. Sugiyama,³⁹ K. Sumisawa,⁹ T. Sumiyoshi,⁵¹ S. Suzuki,³⁹
 S. Y. Suzuki,⁹ O. Tajima,⁹ N. Takada,⁴² F. Takasaki,⁹ K. Tamai,⁹ N. Tamura,³¹

K. Tanabe,⁴⁹ M. Tanaka,⁹ G. N. Taylor,²² Y. Teramoto,³³ X. C. Tian,³⁶ K. Trabelsi,⁸
Y. F. Tse,²² T. Tsuboyama,⁹ T. Tsukamoto,⁹ K. Uchida,⁸ Y. Uchida,⁹ S. Uehara,⁹
T. Uglov,¹³ K. Ueno,²⁸ Y. Unno,⁹ S. Uno,⁹ P. Urquijo,²² Y. Ushiroda,⁹ G. Varner,⁸
K. E. Varvell,⁴⁴ S. Villa,¹⁹ C. C. Wang,²⁸ C. H. Wang,²⁷ M.-Z. Wang,²⁸ M. Watanabe,³¹
Y. Watanabe,⁵⁰ L. Widhalm,¹² C.-H. Wu,²⁸ Q. L. Xie,¹¹ B. D. Yabsley,⁵⁶ A. Yamaguchi,⁴⁸
H. Yamamoto,⁴⁸ S. Yamamoto,⁵¹ Y. Yamashita,³⁰ M. Yamauchi,⁹ Heyoung Yang,⁴¹
J. Ying,³⁶ S. Yoshino,²³ Y. Yuan,¹¹ Y. Yusa,⁴⁸ H. Yuta,¹ S. L. Zang,¹¹ C. C. Zhang,¹¹
J. Zhang,⁹ L. M. Zhang,⁴⁰ Z. P. Zhang,⁴⁰ V. Zhilich,² T. Ziegler,³⁷ and D. Zürcher¹⁹

(The Belle Collaboration)

¹*Aomori University, Aomori*

²*Budker Institute of Nuclear Physics, Novosibirsk*

³*Chiba University, Chiba*

⁴*Chonnam National University, Kwangju*

⁵*University of Cincinnati, Cincinnati, Ohio 45221*

⁶*University of Frankfurt, Frankfurt*

⁷*Gyeongsang National University, Chinju*

⁸*University of Hawaii, Honolulu, Hawaii 96822*

⁹*High Energy Accelerator Research Organization (KEK), Tsukuba*

¹⁰*Hiroshima Institute of Technology, Hiroshima*

¹¹*Institute of High Energy Physics,*

Chinese Academy of Sciences, Beijing

¹²*Institute of High Energy Physics, Vienna*

¹³*Institute for Theoretical and Experimental Physics, Moscow*

¹⁴*J. Stefan Institute, Ljubljana*

¹⁵*Kanagawa University, Yokohama*

¹⁶*Korea University, Seoul*

¹⁷*Kyoto University, Kyoto*

¹⁸*Kyungpook National University, Taegu*

¹⁹*Swiss Federal Institute of Technology of Lausanne, EPFL, Lausanne*

²⁰*University of Ljubljana, Ljubljana*

²¹*University of Maribor, Maribor*

²²*University of Melbourne, Victoria*

²³*Nagoya University, Nagoya*

²⁴*Nara Women's University, Nara*

²⁵*National Central University, Chung-li*

²⁶*National Kaohsiung Normal University, Kaohsiung*

²⁷*National United University, Miao Li*

²⁸*Department of Physics, National Taiwan University, Taipei*

²⁹*H. Niewodniczanski Institute of Nuclear Physics, Krakow*

³⁰*Nippon Dental University, Niigata*

³¹*Niigata University, Niigata*

³²*Nova Gorica Polytechnic, Nova Gorica*

³³*Osaka City University, Osaka*

³⁴*Osaka University, Osaka*

³⁵*Panjab University, Chandigarh*

³⁶*Peking University, Beijing*

³⁷*Princeton University, Princeton, New Jersey 08544*
³⁸*RIKEN BNL Research Center, Upton, New York 11973*
³⁹*Saga University, Saga*

⁴⁰*University of Science and Technology of China, Hefei*

⁴¹*Seoul National University, Seoul*

⁴²*Shinshu University, Nagano*

⁴³*Sungkyunkwan University, Suwon*

⁴⁴*University of Sydney, Sydney NSW*

⁴⁵*Tata Institute of Fundamental Research, Bombay*

⁴⁶*Toho University, Funabashi*

⁴⁷*Tohoku Gakuin University, Tagajo*

⁴⁸*Tohoku University, Sendai*

⁴⁹*Department of Physics, University of Tokyo, Tokyo*

⁵⁰*Tokyo Institute of Technology, Tokyo*

⁵¹*Tokyo Metropolitan University, Tokyo*

⁵²*Tokyo University of Agriculture and Technology, Tokyo*

⁵³*Toyama National College of Maritime Technology, Toyama*

⁵⁴*University of Tsukuba, Tsukuba*

⁵⁵*Utkal University, Bhubaneswer*

⁵⁶*Virginia Polytechnic Institute and State University, Blacksburg, Virginia 24061*

⁵⁷*Yonsei University, Seoul*

Abstract

We report preliminary results of a Dalitz plot analysis of three-body charmless $B^0 \rightarrow K_S^0 \pi^+ \pi^-$ decays. The analysis is performed with a data sample that contains 386 million $B\bar{B}$ pairs collected near the $\Upsilon(4S)$ resonance with the Belle detector at the KEKB asymmetric energy e^+e^- collider. Measurements of branching fractions for quasi-two-body decays $B^0 \rightarrow \rho(770)^0 K^0$, $B^0 \rightarrow f_0(980) K^0$, $B^0 \rightarrow K^*(892)^+ \pi^-$, $B^0 \rightarrow K^*(1430)^+ \pi^-$, and upper limits on several other quasi-two-body decay modes are reported.

PACS numbers: 13.20.He, 13.25.Hw, 13.30.Eg, 14.40.Nd

INTRODUCTION

First results of amplitude analyses of B meson decays to a several three-body charmless hadronic final states have been reported recently: $B^+ \rightarrow K^+K^+K^-$ [1], $B^+ \rightarrow K^+\pi^+\pi^-$ [1, 2, 3], $B^0 \rightarrow K^+\pi^-\pi^0$ [4] and $B^+ \rightarrow \pi^+\pi^+\pi^-$ [3]. Branching fractions for a number of quasi-two-body decays have been measured with some of them being observed for the first time.

In this paper we present preliminary results of a Dalitz plot analysis of neutral B meson decay to the $K_S^0\pi^+\pi^-$ three-body charmless final state. The analysis is based on a 357 fb^{-1} data sample containing 386 million $B\bar{B}$ pairs, collected with the Belle detector operating at the KEKB asymmetric-energy e^+e^- collider [5] with a center-of-mass (c.m.) energy at the $\Upsilon(4S)$ resonance (on-resonance data). The beam energies are 3.5 GeV for positrons and 8.0 GeV for electrons. For the study of the $e^+e^- \rightarrow q\bar{q}$ continuum background, we use data taken 60 MeV below the $\Upsilon(4S)$ resonance (off-resonance data).

THE BELLE DETECTOR

The Belle detector [6] is a large-solid-angle magnetic spectrometer based on a 1.5 T superconducting solenoid magnet. Charged particle tracking is provided by a silicon vertex detector and a 50-layer central drift chamber (CDC) that surround the interaction point. Two inner detector configurations were used. A 2.0 cm beampipe and a 3-layer silicon vertex detector was used for the first sample of 152 million $B\bar{B}$ pairs, while a 1.5 cm beampipe, a 4-layer silicon detector and a small-cell inner drift chamber were used to record the remaining 234 million $B\bar{B}$ pairs [7]. The charged particle acceptance covers laboratory polar angles between $\theta = 17^\circ$ and 150° , corresponding to about 92% of the total solid angle in the c.m. frame. The momentum resolution is determined from cosmic rays and $e^+e^- \rightarrow \mu^+\mu^-$ events to be $\sigma_{p_t}/p_t = (0.30 \oplus 0.19p_t)\%$, where p_t is the transverse momentum in GeV/ c .

Charged hadron identification is provided by dE/dx measurements in the CDC, an array of 1188 aerogel Čerenkov counters (ACC), and a barrel-like array of 128 time-of-flight scintillation counters (TOF); information from the three subdetectors is combined to form a single likelihood ratio, which is then used in kaon and pion selection. Electromagnetic showering particles are detected in an array of 8736 CsI(Tl) crystals (ECL) that covers the same solid angle as the charged particle tracking system. The energy resolution for electromagnetic showers is $\sigma_E/E = (1.3 \oplus 0.07/E \oplus 0.8/E^{1/4})\%$, where E is in GeV. Electron identification in Belle is based on a combination of dE/dx measurements in the CDC, the response of the ACC, and the position, shape and total energy deposition (i.e., E/p) of the shower detected in the ECL. The electron identification efficiency is greater than 92% for tracks with $p_{\text{lab}} > 1.0 \text{ GeV}/c$ and the hadron misidentification probability is below 0.3%. The magnetic field is returned via an iron yoke that is instrumented to detect muons and K_L^0 mesons. We use a GEANT-based Monte Carlo (MC) simulation to model the response of the detector and determine its acceptance [8].

EVENT RECONSTRUCTION

Charged tracks are selected with a set of track quality requirements based on the number of CDC hits and on the distances of closest approach to the interaction point. We also

require that the track momenta transverse to the beam be greater than 0.1 GeV/ c to reduce the low momentum combinatorial background. Charged tracks that are positively identified as kaons, protons or electrons are excluded. Since the muon identification efficiency and fake rate vary significantly with the track momentum, we do not veto muons to avoid additional systematic errors.

We identify B candidates using two variables: the difference ΔE between the total reconstructed energy of a three-body combination and the nominal beam energy in the c.m. frame and the beam constrained mass M_{bc} . ΔE is calculated as $\Delta E = E_B - E_{\text{beam}}^* = \left(\sum_i \sqrt{c^2 \mathbf{p}_i^2 + c^4 m_i^2} \right) - E_{\text{beam}}^*$, where the summation is over all particles from a B candidate; and \mathbf{p}_i and m_i are their c.m. three-momenta and masses, respectively. Since there are no π^0 's or photons in the final state, the ΔE width (with typical value of 15 MeV) is governed by the track momentum resolution. The beam energy spread is about 3 MeV and gives a negligible contribution to the total ΔE width. The signal ΔE shape is parametrized by a sum of two Gaussian functions with a common mean. The ΔE shape for the $q\bar{q}$ background is parametrized by a linear function. The beam constrained mass variable M_{bc} is equivalent to the B invariant mass with the measured B candidate energy E_B replaced by the beam energy E_{beam}^* : $M_{bc} = \frac{1}{c^2} \sqrt{E_{\text{beam}}^{*2} - c^2 \mathbf{P}_B^2} = \frac{1}{c^2} \sqrt{E_{\text{beam}}^{*2} - c^2 (\sum_i \mathbf{p}_i)^2}$, where \mathbf{P}_B is the B candidate momentum in the c.m. frame. The average B meson momentum in the c.m. frame is about 0.34 GeV/ c which is much smaller than its total energy. Thus, the uncertainty in the measured \mathbf{P}_B gives a small contribution to the M_{bc} width, which is dominated by the beam energy spread. The M_{bc} width is about 3 MeV/ c^2 and well described by a single Gaussian function. The M_{bc} width in general, does not depend on the final state (unless photons are included in the reconstructed final state).

BACKGROUND SUPPRESSION

There are two sources of the background: the dominant one is due to $e^+e^- \rightarrow q\bar{q}$ ($q = u, d, s$ and c quarks) continuum events that have a cross-section about three times larger than that for the $e^+e^- \rightarrow \Upsilon(4S) \rightarrow B\bar{B}$; the other one originates from other B meson decays. The background from continuum events is suppressed using variables that characterize the event topology. Since the two B mesons produced from an $\Upsilon(4S)$ decay are nearly at rest in the c.m. frame, their decay products are uncorrelated and the event tends to be spherical. In contrast, hadrons from continuum $q\bar{q}$ events tend to exhibit a two-jet structure. We use θ_{thr} , which is the angle between the thrust axis of the B candidate and that of the rest of the event, to discriminate between the two cases. The distribution of $|\cos \theta_{\text{thr}}|$, is strongly peaked near $|\cos \theta_{\text{thr}}| = 1.0$ for $q\bar{q}$ events and is nearly flat for $B\bar{B}$ events. We require $|\cos \theta_{\text{thr}}| < 0.80$ eliminating about 83% of the continuum background and retaining 79% of the signal events. For further suppression of the continuum background we use a Fisher discriminant formed from 11 variables: nine variables that characterize the angular distribution of the momentum flow in the event with respect to the B candidate thrust axis, the angle of the B candidate thrust axis with respect to the beam axis, and the angle between the B candidate momentum and the beam axis. The discriminant, \mathcal{F} , is the linear combination of the input variables that maximizes the separation between signal and background. The coefficients are determined using off-resonance data and a large set of signal MC events. Use of the Fisher discriminant rejects about 89% of the remaining continuum background with 53% efficiency for the signal. A more detailed description of

the background suppression technique can be found in Ref. [9] and references therein.

The understanding of the background that originates from other B meson decays is of great importance in the study of charmless B decays. We study the $B\bar{B}$ related background using a large sample of MC generated $B\bar{B}$ generic events. We find that the dominant $B\bar{B}$ related background is due to $B^0 \rightarrow D^-\pi^+$, $D^- \rightarrow K_S^0\pi^-$ and due to $B^0 \rightarrow J/\psi(\psi(2S))K_S^0$, $J/\psi(\psi(2S)) \rightarrow \mu^+\mu^-$ decays. We veto $B^0 \rightarrow D^-\pi^+$ events by requiring $|M(K_S^0\pi) - M_D| > 100 \text{ MeV}/c^2$. Modes with $J/\psi(\psi(2S))$ contribute due to muon-pion misidentification; the contribution from the $J/\psi(\psi(2S)) \rightarrow e^+e^-$ submode is found to be negligible after the electron veto requirement. We exclude $J/\psi(\psi(2S))$ background by requiring $|M(\pi^+\pi^-)_{\mu^+\mu^-} - M_{J/\psi}| > 70 \text{ MeV}/c^2$ and $|M(\pi^+\pi^-)_{\mu^+\mu^-} - M_{\psi(2S)}| > 50 \text{ MeV}/c^2$, with a muon mass assignment used here for the pion candidates. To suppress the background due to K/π misidentification, we also exclude candidates if the invariant mass of any pair of oppositely charged tracks from the B candidate is consistent with the $D^+ \rightarrow K_S^0K^+$ hypothesis within $15 \text{ MeV}/c^2$ ($\sim 2.5\sigma$), regardless of the particle identification information. The most significant background from charmless B decays is found to originate from the decay $B^0 \rightarrow \eta'K_S^0$ followed by $\eta' \rightarrow \pi^+\pi^-\gamma$. There is also a contribution from the two-body charmless decay $B^\pm \rightarrow K_S^0\pi^\pm$. Although this background is shifted by about 0.2 GeV from the ΔE signal region, it is important to take it into account for correct estimation of the background from continuum events.

THREE-BODY SIGNAL YIELDS

The ΔE distributions for $B^0 \rightarrow K_S^0\pi^+\pi^-$ candidates that pass all the selection requirements are shown in Fig. 1(a), where clear peak in the signal region is observed. The two dimensional ΔE versus M_{bc} plot is shown in Fig. 1(b). In the fit to the ΔE distribution we fix the shape and normalization of the charmless $B\bar{B}$ background components from their measured branching fractions [10] and known number of produced $B\bar{B}$ events. For the $B\bar{B}$ generic component we fix only the shape and let the normalization float. The slope and normalization of the $q\bar{q}$ background component are free parameters. For signal we fix the width of the second Gaussian function at 31.0 MeV and the fraction at 0.19 as determined from MC simulation. The width of the main Gaussian is floating. The fit finds 1229 ± 62 signal events. The sigma of the main Gaussian is $15.3 \pm 0.9 \text{ MeV}$. Results of the fit are shown in Fig. 1(a), where different components of the background are shown separately for comparison. There is a large increase in the level of the $B\bar{B}$ related background in $\Delta E < -0.15 \text{ GeV}$ region. This is mainly due to $B \rightarrow D\pi$, $D \rightarrow K\pi\pi$ decay. This decay mode produces the same final state as the studied process plus one extra pion that is not included in the energy difference calculation. The semileptonic decays $B \rightarrow D^{(*)}\pi$, $D \rightarrow K\mu\nu_\mu$ also contribute due to muon-pion misidentification. The shape of the $B\bar{B}$ background is described well by MC simulation.

To examine possible quasi-two-body intermediate states in the observed $B^0 \rightarrow K_S^0\pi^+\pi^-$ signal, we analyze the two-particle invariant mass spectra. To do so we define the B signal and sideband regions as illustrated in Fig. 1(c). Defined in this way, the $M_{bc} - \Delta E$ sidebands are equivalent to the following sidebands in terms of the three-particle invariant mass $M(K\pi\pi)$ and three-particle momentum $P(K\pi\pi)$:

$$0.05 \text{ GeV}/c^2 < |M(K\pi\pi) - M_B| < 0.10 \text{ GeV}/c^2; \quad P(K\pi\pi) < 0.48 \text{ GeV}/c$$

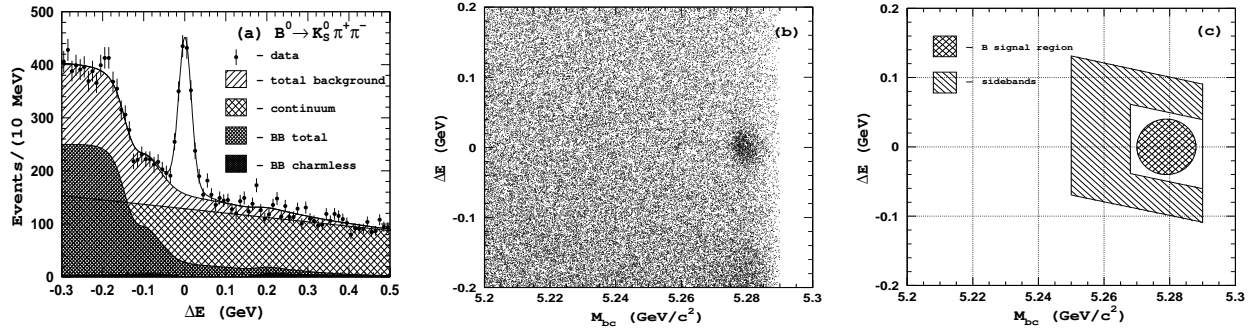


FIG. 1: ΔE distribution for the $B^0 \rightarrow K_S^0 \pi^+ \pi^-$ candidate events with $|M_{bc} - M_B| < 7.5 \text{ MeV}/c^2$. Points with error bars are data; the upper curve is the fit result; the hatched histogram is the background. (b) Distribution of ΔE versus M_{bc} for the $B^0 \rightarrow K_S^0 \pi^+ \pi^-$ candidates in data. (c) Definition of the B signal and sideband regions in the $M_{bc} - \Delta E$ plane.

and

$$|M(K\pi\pi) - M_B| < 0.10 \text{ GeV}/c^2; \quad 0.48 \text{ GeV}/c < P(K\pi\pi) < 0.65 \text{ GeV}/c.$$

The B signal region is defined as an ellipse around the M_{bc} and ΔE mean values:

$$\frac{(M_{bc} - M_B)^2}{(7.5 \text{ MeV}/c^2)^2} + \frac{\Delta E^2}{(40 \text{ MeV})^2} < 1.$$

The efficiency of the requirements that define the signal region is 0.923. The total number of events in the signal region is 2207. The relative fraction of signal events in the B signal region is then determined to be 0.521 ± 0.025 .

The $K_S^0 \pi^\pm$ and $\pi^+ \pi^-$ invariant mass spectra for $B^0 \rightarrow K_S^0 \pi^+ \pi^-$ candidate events in the B signal region are shown as open histograms in Fig. 2. The hatched histograms show the corresponding spectra for background events in the $M_{bc} - \Delta E$ sidebands, normalized to the estimated number of background events. To suppress the feed-across between the $\pi^+ \pi^-$ and $K_S^0 \pi^\pm$ resonance states, we require the $K_S^0 \pi^\pm$ ($\pi^+ \pi^-$) invariant mass to be larger than $1.5 \text{ GeV}/c^2$ when making the $\pi^+ \pi^-$ ($K_S^0 \pi^\pm$) projection. The $K_S^0 \pi^\pm$ invariant mass spectrum is characterized by a narrow peak around $0.9 \text{ GeV}/c^2$ which is identified as the $K^*(892)^\pm$ and a broad enhancement around $1.4 \text{ GeV}/c^2$. Possible candidates to assign to this enhancement are the scalar $K_0^*(1430)^\pm$ and tensor $K_2^*(1430)^\pm$ resonances. In the $\pi^+ \pi^-$ invariant mass spectrum three distinct structures in the low mass region are observed. The most prominent one is slightly below $1.0 \text{ GeV}/c^2$ and is consistent with the $f_0(980)$. There is a clear indication for the $\rho(770)^0$ signal to the left of the $f_0(980)$ peak. Finally, there is a less prominent structure between $1.2 \text{ GeV}/c^2$ and $1.5 \text{ GeV}/c^2$. We cannot identify unambiguously the resonance state that is responsible for such a structure; possible candidates for a resonance state in this mass region might be $f_0(1370)$, $f_2(1270)$ and perhaps $\rho(1450)$ [10]. In what follows, we refer to this structure as $f_X(1300)$. It is worth noting that both $K\pi$ and $\pi\pi$ two-body spectra in three-body $B^0 \rightarrow K_S^0 \pi^+ \pi^-$ decays are similar to those observed in charged B meson decay to the three-body $K^+ \pi^+ \pi^-$ final state [1]. As we observe a clear $B^+ \rightarrow \chi_{c0} K^+$ signal in the analysis of $B^+ \rightarrow K^+ \pi^+ \pi^-$ decay, we expect $B^0 \rightarrow \chi_{c0} K^0$ decay to occur at a similar rate. However, the $\pi^+ \pi^-$ mass spectrum for the χ_{c0} region shown in Fig. 2(c) does not reveal the χ_{c0} signal clearly.

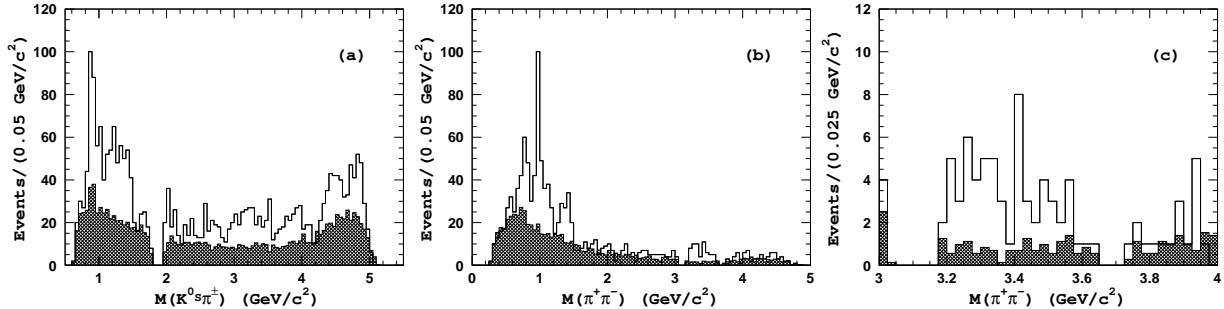


FIG. 2: Two-particle invariant mass spectra for the $B^0 \rightarrow K_S^0 \pi^+ \pi^-$ candidates in the B signal region (open histograms) and for background events in the $\Delta E - M_{bc}$ sidebands (hatched histograms). (a) $M(K_S^0 \pi^\pm)$ spectrum with $M(\pi^+ \pi^-) > 1.5 \text{ GeV}/c^2$ (note that there are two entries per candidate in this plot); (b) $M(\pi^+ \pi^-)$ with $M(K_S^0 \pi^\pm) > 1.5 \text{ GeV}/c^2$ and (c) $M(\pi^+ \pi^-)$ in the χ_{c0} mass region with $M(K_S^0 \pi^\pm) > 1.5 \text{ GeV}/c^2$.

From these qualitative considerations it is apparent that an amplitude analysis is required for a more complete understanding of the individual quasi-two-body channels that contribute to the observed three-body $B^0 \rightarrow K_S^0 \pi^+ \pi^-$ signal.

AMPLITUDE ANALYSIS

In the preceding section we found that a significant fraction of the $B^0 \rightarrow K_S^0 \pi^+ \pi^-$ signal can be assigned to quasi-two-body intermediate states. These resonances will cause a non-uniform distribution of events in phase space that can be analyzed using the technique pioneered by Dalitz [11]. Multiple resonances that occur nearby in phase space will interfere providing an opportunity to measure their amplitudes and relative phases. This in turn allows us to deduce their relative fractions.

The amplitude analysis of B meson three-body decays reported here is performed by means of an unbinned maximum likelihood fit. As the unbinned maximum likelihood fitting method does not provide a direct way to estimate the quality of the fit, we need a measure to assess how well any given fit represents the data. To do so the following procedure is applied. We first subdivide the entire Dalitz plot into $1 (\text{GeV}/c^2)^2 \times 1 (\text{GeV}/c^2)^2$ bins. If the number of events in the bin is smaller than $N_{\min} = 16$ it is combined with the adjacent bins until the number of events exceeds N_{\min} . After completing this procedure, the entire Dalitz plot is divided into a set of bins of varying size, and a χ^2 variable for the multinomial distribution can be calculated as

$$\chi^2 = -2 \sum_{i=1}^{N_{\text{bins}}} n_i \ln \left(\frac{p_i}{n_i} \right), \quad (1)$$

where n_i is the number of events observed in the i -th bin, and p_i is the number of predicted events from the fit. For a large number of events this formulation becomes equivalent to the usual one. Since we are minimizing the unbinned likelihood function, our “ χ^2 ” variable does not asymptotically follow a χ^2 distribution but it is bounded by a χ^2 variable with $(N_{\text{bins}} - 1)$ degrees of freedom and a χ^2 variable with $(N_{\text{bins}} - k - 1)$ degrees of freedom [12], where k is the number of fit parameters. Because it is bounded by two χ^2 variables, it should

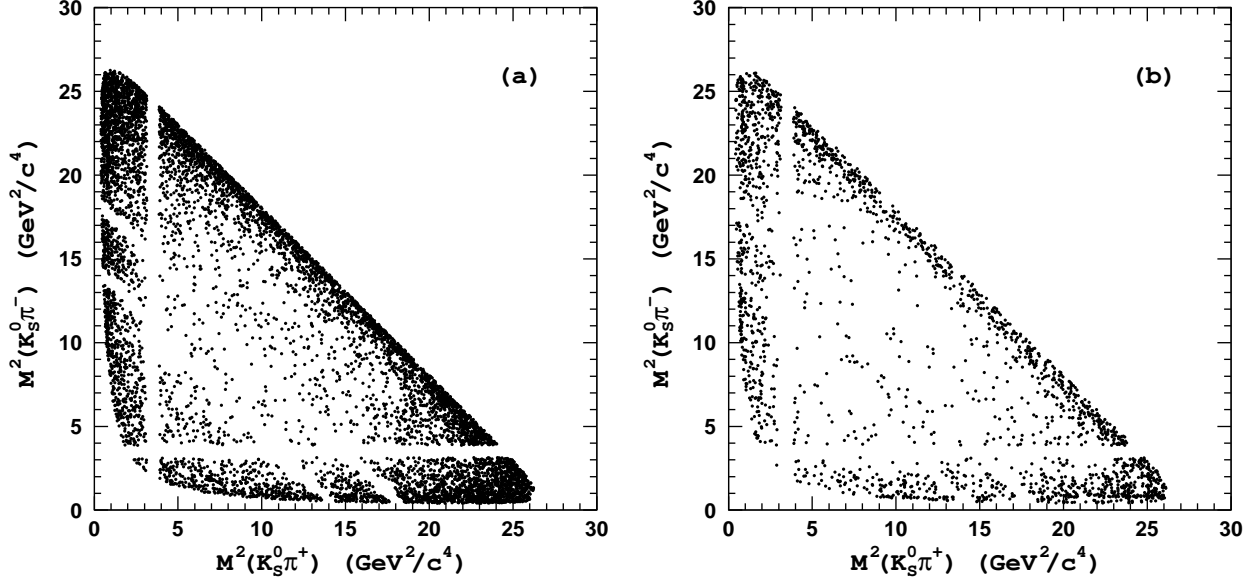


FIG. 3: Dalitz plots for $K_S^0\pi^+\pi^-$ candidates in the (a) $\Delta E - M_{bc}$ sidebands and (b) B signal region.

be a useful statistic for comparing the relative goodness of fits for different models. A more detailed description of the technique is given in Ref. [1].

Fitting the Background Shape

Before fitting the Dalitz plot for events in the signal region, we need to determine the distribution of background events. The background density function is determined from an unbinned likelihood fit to the events in the $M_{bc} - \Delta E$ sidebands defined in Fig. 1(c). Figure 3(a) shows Dalitz distribution for 8159 sideband events. This is about seven times the estimated number of background events in the B signal region.

We use the following empirical parametrization to describe the distribution of background events over the Dalitz plot in the $K_S^0\pi^+\pi^-$ final state

$$\begin{aligned}
 B(s_{13}, s_{23}) = & \alpha_1(e^{-\beta_1 s_{12}} + e^{-\beta_1 s_{13}}) + \alpha_2 e^{-\beta_2 s_{23}} \\
 & + \alpha_3(e^{-\beta_3 s_{12} - \beta_4 s_{23}} + e^{-\beta_3 s_{13} - \beta_4 s_{23}}) + \alpha_4 e^{-\beta_5 (s_{12} + s_{13})} \\
 & + \gamma_1(|BW(K^*(892)^-)|^2 + |BW(K^*(892)^+)|^2) + \gamma_2|BW(\rho(770)^0)|^2, \quad (2)
 \end{aligned}$$

where $s_{12} \equiv M^2(K_S^0\pi^-)$, $s_{13} \equiv M^2(K_S^0\pi^+)$, $s_{23} \equiv M^2(\pi^+\pi^-)$ and α_i ($\alpha_1 \equiv 1.0$), β_i and γ_i are fit parameters; BW is a Breit-Wigner function. The first three terms in Eq. (2) are introduced to describe the background enhancement in the two-particle low invariant mass regions. This enhancement originates mainly from $e^+e^- \rightarrow q\bar{q}$ continuum events. Due to the jet-like structure of this background, all three particles in a three-body combination have almost collinear momenta. Hence, the invariant mass of at least one pair of particles is in the low mass region. In addition, it is often the case that two high momentum particles are combined with a low momentum particle to form a B candidate. In this case there are two pairs with low invariant masses and one pair with high invariant mass resulting in even

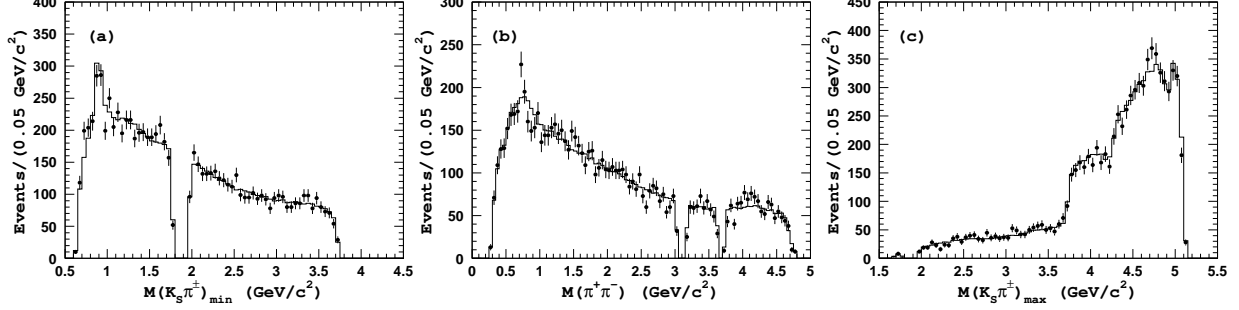


FIG. 4: Results of the best fit to the $K_S^0 \pi^+ \pi^-$ events in the $\Delta E - M_{bc}$ sidebands shown as projections onto two-particle invariant mass variables. Points with error bars are data; histograms are fit results.

stronger enhancement of the background in the corners of the Dalitz plot. This is taken into account by terms 4 – 6 in Eq. (2). To account for the contribution from real $K^*(892)^\pm$ and $\rho(770)^0$ mesons, we introduce two more terms in Eq. (2), that are (non-interfering) squared Breit-Wigner amplitudes, with masses and widths fixed at world average values [10]. The projections of the data and fits for the background events are shown in Figs. 4. The χ^2/N_{bins} value of the fit is 241.7/197.

Fitting the Signal

The Dalitz plot for $K_S^0 \pi^+ \pi^-$ events in the signal region is shown in Fig. 3(b). There are 2207 events in the signal region that satisfy all the selection requirements. In an attempt to describe all the features of the $K_S^0 \pi^\pm$ and $\pi^+ \pi^-$ mass spectra mentioned above, we use matrix element (referred to as model $K\pi\pi - C_J$) similar to those constructed in the analysis of $B^+ \rightarrow K^+ \pi^+ \pi^-$ decay [1]:

$$\begin{aligned}
\mathcal{M}_{C_J}(K_S^0 \pi^+ \pi^-) = & a_{K^*} e^{i\delta_{K^*}} \mathcal{A}_1(\pi^+ K_S^0 \pi^- | K^*(892)^+) + a_{K_0^*} e^{i\delta_{K_0^*}} \mathcal{A}_0(\pi^+ K_S^0 \pi^- | K_0^*(1430)^+) \\
& + a_\rho e^{i\delta_\rho} \mathcal{A}_1(K_S^0 \pi^+ \pi^- | \rho(770)^0) + a_{f_0} e^{i\delta_{f_0}} \mathcal{A}_{\text{Flatte}}(K_S^0 \pi^+ \pi^- | f_0(980)) \\
& + a_{f_X} e^{i\delta_{f_X}} \mathcal{A}_J(K_S^0 \pi^+ \pi^- | f_X(1300)) + a_{\chi_{c0}} e^{i\delta_{\chi_{c0}}} \mathcal{A}_0(K_S^0 \pi^+ \pi^- | \chi_{c0}) \\
& + \mathcal{A}_{\text{nr}}(K_S^0 \pi^+ \pi^-),
\end{aligned} \tag{3}$$

where the subscript J denotes the unknown spin of the $f_X(1300)$ resonance; amplitudes a_i , relative phases δ_i , are fit parameters. The masses and widths of all resonances are fixed at either their world average values [10] or at values determined from the analysis of $B^+ \rightarrow K^+ \pi^+ \pi^-$ decay ($f_0(980)$ and $f_X(1300)$). The $f_0(980)$ is parametrized with a coupled channel Breit-Wigner function (Flatte parametrization [13]). For the non-resonant amplitude \mathcal{A}_{nr} we use an empirical parametrization

$$\mathcal{A}_{\text{nr}}(K_S^0 \pi^+ \pi^-) = a_1^{\text{nr}} e^{-\alpha s_{13}} e^{i\delta_1^{\text{nr}}} + a_2^{\text{nr}} e^{-\alpha s_{23}} e^{i\delta_2^{\text{nr}}}. \tag{4}$$

Finally, as we currently do not perform the flavor analysis of the other B meson, we cannot distinguish whether a B or \bar{B} meson decays to the $K_S^0 \pi^+ \pi^-$ final state. Thus the signal PDF is a non-coherent sum

$$S_{C_J}(K_S^0 \pi^+ \pi^-) = |\mathcal{M}_{C_J}(K_S^0 \pi^+ \pi^-)|^2 + |\mathcal{M}_{C_J}(K_S^0 \pi^- \pi^+)|^2. \tag{5}$$

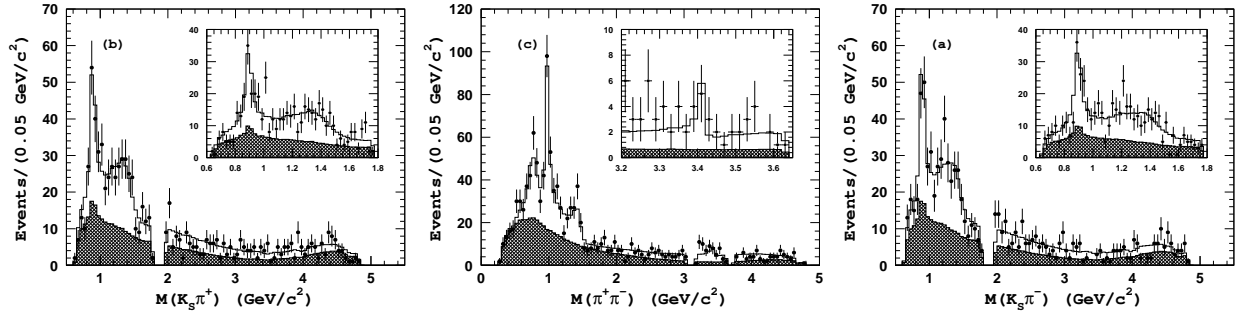


FIG. 5: Results of the fit to $K_S^0 \pi^+ \pi^-$ events in the signal region with the model $K \pi \pi - C_0$. Points with error bars are data, the open histograms are the fit result and hatched histograms are the background components. Insets in (a) and (b) show the $K^*(892) - K_0^*(1430)$ mass region in $20 \text{ MeV}/c^2$ bins; inset in (c) shows the χ_{c0} mass region in $25 \text{ MeV}/c^2$ bins.

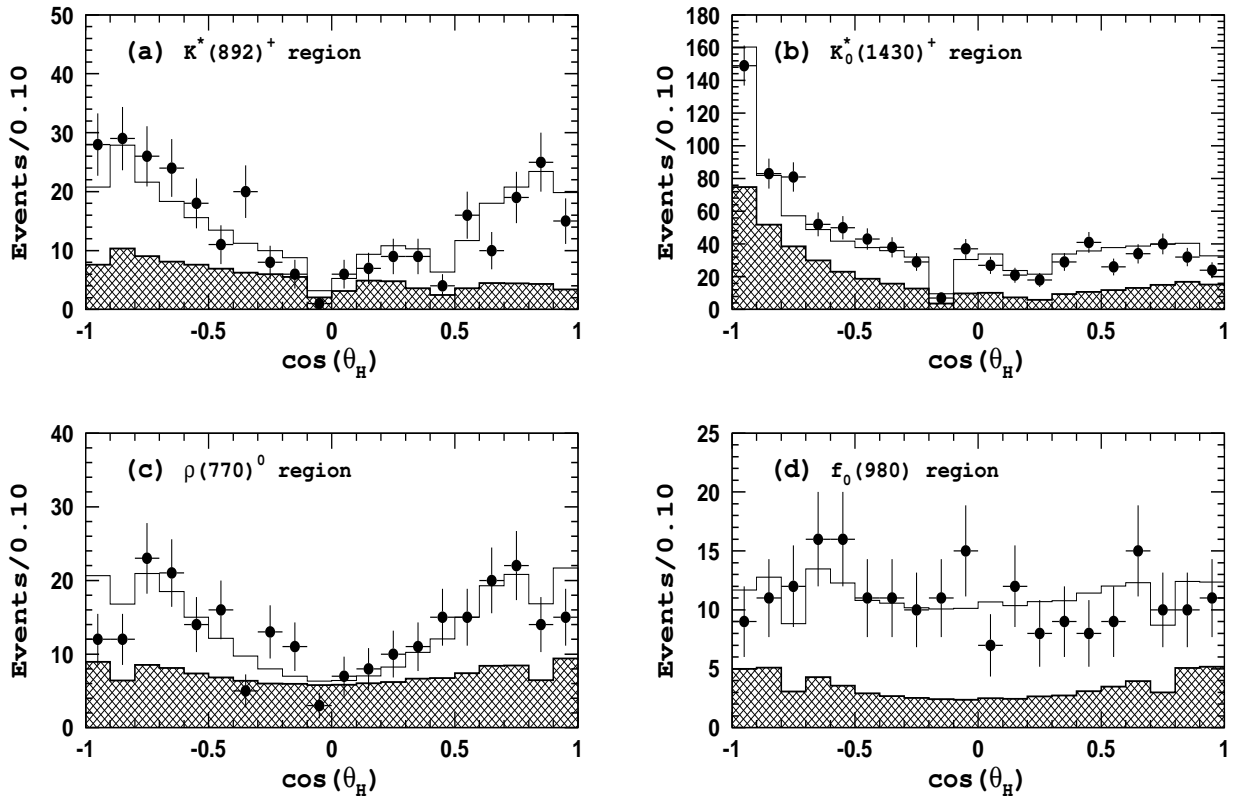


FIG. 6: Helicity angle distributions for $K_S^0 \pi^+ \pi^-$ events in different regions:

(a) $K^*(892)^+$ ($0.82 \text{ GeV}/c^2 < M(K_S^0 \pi^\pm) < 0.97 \text{ GeV}/c^2$);

(b) $K_0^*(1430)^+$ ($1.0 \text{ GeV}/c^2 < M(K^+ \pi^-) < 1.76 \text{ GeV}/c^2$);

(c) $\rho(770)^0$ ($M(\pi^+ \pi^-) < 0.90 \text{ GeV}/c^2$);

(d) $f_0(980)$ ($0.90 \text{ GeV}/c^2 < M(\pi^+ \pi^-) < 1.06 \text{ GeV}/c^2$). Points with error bars are data, the open histogram is the fit result and the hatched histogram is the background component. Note that in plots (a) and (b) there are two entries per B candidate.

TABLE I: Results of the fit to $K_S^0\pi^+\pi^-$ events in the B signal region with model $K\pi\pi-C_0$. The first quoted error is statistical and the second is the model dependent uncertainty.

| Mode | Parameter | | | |
|----------------------|--|---|----------------------|--|
| | Fraction, % | Phase, $^\circ$ | Mass, GeV/ c^2 | Width, GeV/ c^2 |
| $K^*(892)^+\pi^-$ | $11.8 \pm 1.4 \pm_{-0.6}^{+0.9}$ | 0 (fixed) | 0.89166 (fixed) [10] | 0.0508 (fixed) [10] |
| $K_0^*(1430)^+\pi^-$ | $64.8 \pm 3.9 \pm_{-6.3}^{+1.6}$ | $45 \pm 9 \pm_{-13}^{+9}$ | 1.412 (fixed) [10] | 0.294 (fixed) [10] |
| $\rho(770)^0 K^0$ | $12.9 \pm 1.9 \pm_{-2.2}^{+2.1}$ | $-9 \pm 28 \pm_{-13}^{+27}$ | 0.7758 (fixed) [10] | 0.1503 (fixed) [10] |
| $f_0(980)K^0$ | $16.0 \pm 3.4 \pm_{-1.4}^{+1.0}$ | $36 \pm 34 \pm_{-21}^{+38}$ | 0.950 (fixed) [2] | $g_{\pi\pi} = 0.23$ (fixed) [2] $g_{KK} = 0.73$ (fixed) [2] |
| $\chi_{c0}K^0$ | $0.43 \pm_{-0.17}^{+0.42} \pm_{-0.06}^{+0.02}$ | $-99 \pm 37 \pm_{-8}^{+8}$ | 3.415 (fixed) [10] | 0.011 (fixed) [10] |
| $f_X(1300)K^0$ | $3.68 \pm 2.16 \pm_{-0.49}^{+0.53}$ | $-135 \pm 25 \pm_{-26}^{+24}$ | 1.449 (fixed) [2] | 0.126 (fixed) [2] |
| Non-Resonant | $41.9 \pm 5.1 \pm_{-2.5}^{+1.4}$ | $\delta_1^{\text{nr}} = -22 \pm 8 \pm_{-6}^{+6}$ $\delta_2^{\text{nr}} = 175 \pm 30 \pm_{-30}^{+54}$ | — | — |
| Charmless Only | $99.3 \pm 0.4 \pm 0.1$ | — | — | — |

While fitting the data, we choose the $K^*(892)^+\pi^-$ signal as our reference by fixing its amplitude and phase ($a_{K^*} \equiv 1$ and $\delta_{K^*} \equiv 0$). The numerical values of the fit parameters are given in Table I. Figure 5 shows the fit projections and the data. In addition, helicity angle distributions for several regions are shown in Fig. 6. The helicity angle is defined as the angle between the direction of flight of the π^+ (π^-) in the $K_S^0\pi^+$ ($K_S^0\pi^-$) rest frame and the direction of $K_S^0\pi$ system in the B rest frame. For the $\pi^+\pi^-$ system the helicity angle is defined with respect to the positively charged pion. Gaps visible in Figs. 5 and 6 are due to vetoes applied on invariant masses of two-particle combinations. All plots shown in Figs. 5 and 6 demonstrate good agreement between data and the fit. We also try to fit the data assuming $f_X(1300)$ is a vector (tensor) state. In this case we ascribe mass and width of $\rho(1450)$ ($f_2(1270)$) from PDG [10] to it. If parametrized by a single resonant state the best fit is achieved with a scalar assumption.

MODEL & SYSTEMATIC UNCERTAINTIES

To estimate the model dependent uncertainty and test for the contribution of other possible quasi-two-body intermediate states such as $K^*(1410)^+\pi^-$, $K^*(1680)^+\pi^-$, $K_2^*(1430)^+\pi^-$ or $f_2(1270)K^0$, we include an additional amplitude of either of these channels to model $K\pi\pi-C_0$ and repeat the fit to data. For none of these channels is a statistically significant signal found. We also use several alternative (though also empirical) parametrizations of the non-resonant amplitude to estimate the related uncertainty

- $\mathcal{A}_{\text{nr}}(K_S^0\pi^+\pi^-) = a_1^{\text{nr}} e^{-\alpha s_{13}} e^{i\delta_1^{\text{nr}}}$;
- $\mathcal{A}_{\text{nr}}(K_S^0\pi^+\pi^-) = a_1^{\text{nr}} e^{-\alpha s_{13}} e^{i\delta_1^{\text{nr}}} + a_2^{\text{nr}} e^{-\alpha s_{23}} e^{i\delta_2^{\text{nr}}} + a_3^{\text{nr}} e^{-\alpha s_{12}} e^{i\delta_3^{\text{nr}}}$;
- $\mathcal{A}_{\text{nr}}(K_S^0\pi^+\pi^-) = \frac{a_1^{\text{nr}}}{s_{13}^\alpha} e^{i\delta_1^{\text{nr}}} + \frac{a_2^{\text{nr}}}{s_{23}^\alpha} e^{i\delta_2^{\text{nr}}}$.

The dominant sources of systematic error are listed in Table II. For the branching fraction of the three-body $B^0 \rightarrow K_S^0\pi^+\pi^-$ decay, we estimate the systematic uncertainty due to

TABLE II: List of systematic errors (in percent) for the three-body $B^0 \rightarrow K_S^0 \pi^+ \pi^-$ branching fraction.

| Source | Error |
|------------------------------|-------|
| Charged track reconstruction | 2.0 |
| PID | 2.0 |
| K_S^0 reconstruction | 3.0 |
| Event Shape requirements | 2.5 |
| Signal yield extraction | 5.4 |
| Model | 2.2 |
| MC statistics | 1.0 |
| Luminosity measurement | 1.0 |
| Total | 7.7 |

possible losses from the mass cuts used to remove contributions from charmed particles by varying the relative phases and amplitudes of the quasi-two-body states within their errors. The systematic uncertainty due to requirements on event shape variables is estimated from a comparison of the $|\cos\theta_{\text{thr}}|$ and \mathcal{F} distributions for signal MC events and $B^+ \rightarrow \bar{D}^0 \pi^+$ events in the data. The uncertainty from the particle identification efficiency is estimated using pure samples of kaons and pions from the $D^0 \rightarrow K^- \pi^+$ decays, where the D^0 flavor is tagged using $D^{*+} \rightarrow D^0 \pi^+$ decays. We estimate the uncertainty due to the signal ΔE shape parameterization by varying the parameters of the fitting function within their errors. The uncertainty in the background parameterization is estimated by varying the relative fraction of the $B\bar{B}$ background component and the slope of the $q\bar{q}$ background function within their errors. The overall systematic uncertainty for the three-body branching fraction is estimated to be $\pm 7.7\%$.

RESULTS

In previous sections we determined the relative fractions of various quasi-two-body intermediate states in the three-body $B^0 \rightarrow K_S^0 \pi^+ \pi^-$ decay. To translate these numbers into absolute branching fractions, we first need to determine the branching fractions for the three body decay. To determine the reconstruction efficiency for the $B^0 \rightarrow K_S^0 \pi^+ \pi^-$ decay, we use MC simulation where events are distributed over the phase space according to the matrix elements of the model $K\pi\pi-C_0$. The corresponding reconstruction efficiency is $6.71 \pm 0.03\%$ (including $K^0 \rightarrow \pi^+ \pi^-$ fraction).

Results of the branching fraction calculations are summarized in Table III. For final states where no statistically significant signal is observed we calculate 90% confidence level upper limits f_{90} for their fractions. To determine the upper limit we use the following formula

$$0.90 = \frac{\int_0^{f_{90}} G(a, s; x) dx}{\int_0^\infty G(a, s; x) dx}, \quad (6)$$

where $G(a, s; x)$ is a Gaussian function with mean a and sigma s which are the measured mean value for the signal fraction and its statistical error. To account for the systematic uncertainty we decrease the reconstruction efficiency by one standard deviation.

TABLE III: Summary of branching fraction results. The first quoted error is statistical, the second is systematic and the third is the model error.

| Mode | $\mathcal{B}(B \rightarrow Rh) \times \mathcal{B}(R \rightarrow hh) \times 10^6$ | $\mathcal{B}(B \rightarrow Rh) \times 10^6$ |
|---|--|---|
| $K_S^0 \pi^+ \pi^-$ charmless total | | $47.5 \pm 2.4 \pm 3.7$ |
| $K^*(892)^+ \pi^-$, $K^*(892)^+ \rightarrow K^0 \pi^+$ | $5.61 \pm 0.72 \pm 0.43_{-0.29}^{+0.43}$ | $8.42 \pm 1.08 \pm 0.65_{-0.43}^{+0.64}$ |
| $K_0^*(1430)^+ \pi^-$, $K_0^*(1430)^+ \rightarrow K^0 \pi^+$ | $30.8 \pm 2.4 \pm 2.4_{-3.0}^{+0.8}$ | $49.7 \pm 3.8 \pm 3.8_{-4.8}^{+1.2}$ |
| $K^*(1410)^+ \pi^-$, $K^*(1410)^+ \rightarrow K^0 \pi^+$ | < 3.8 | – |
| $K^*(1680)^+ \pi^-$, $K^*(1680)^+ \rightarrow K^0 \pi^+$ | < 2.6 | – |
| $K_2^*(1430)^+ \pi^-$, $K_2^*(1430)^+ \rightarrow K^0 \pi^+$ | < 2.1 | – |
| $\rho(770)^0 K^0$, $\rho(770)^0 \rightarrow \pi^+ \pi^-$ | $6.13 \pm 0.95 \pm 0.47_{-1.05}^{+1.00}$ | $6.13 \pm 0.95 \pm 0.47_{-1.05}^{+1.00}$ |
| $f_0(980) K^0$, $f_0(980) \rightarrow \pi^+ \pi^-$ | $7.60 \pm 1.66 \pm 0.59_{-0.67}^{+0.48}$ | – |
| $f_2(1270) K^0$, $f_2(1270) \rightarrow \pi^+ \pi^-$ | < 1.4 | – |
| Non-resonant | | $19.9 \pm 2.5 \pm 1.5_{-1.2}^{+0.7}$ |
| $\chi_{c0} K^0$, $\chi_{c0} \rightarrow \pi^+ \pi^-$ | < 0.56 | < 113 |

DISCUSSION & CONCLUSION

With a 357 fb^{-1} data sample collected with the Belle detector, an amplitude (Dalitz) analysis of B meson decays to three-body charmless $K_S^0 \pi^+ \pi^-$ final states is performed for the first time. Clear signals are observed in the $B^0 \rightarrow K^*(892)^+ \pi^-$, $B^0 \rightarrow K_0^*(1430)^+ \pi^-$, $B^0 \rightarrow \rho(770)^0 K^0$ and $B^0 \rightarrow f_0(980) K^0$ decay channels. The model uncertainty for these channels is small due to their narrow width and, for vector-pseudoscalar decays, due to clear signature because of the 100% polarization of the vector meson. Among these quasi-two-body channels the decay $B^0 \rightarrow \rho(770)^0 K^0$ is observed for the first time.

The branching fraction measured for the decay $B^0 \rightarrow K^*(892)^+ \pi^-$ is in agreement with results from the amplitude analysis of the three-body $B^0 \rightarrow K^+ \pi^- \pi^0$ decay [4, 14], where the $K^*(892)^+$ is reconstructed in the $K^+ \pi^0$ channel.

We also check possible contributions from $B^0 \rightarrow K_2^*(1430)^+ \pi^-$, $B^0 \rightarrow K^*(1410)^+ \pi^-$, $B^0 \rightarrow K^*(1680)^+ \pi^-$ and $B^0 \rightarrow f_2(1270) K^0$ decays. We find no statistically significant signal in any of these channels and set 90% confidence level upper limits for their branching fractions. In the factorization approximation, charmless B decays to final states with a tensor state are expected to occur at the level of $\sim 10^{-7}$ [15].

We cannot identify unambiguously the broad structures observed in the $M(\pi^+ \pi^-) \simeq 1.3 \text{ GeV}/c^2$ mass region. If approximated by a single resonant state, the best description is achieved with a scalar amplitude whose mass and width are consistent with those for the $f_0(1370)$. Because of the large uncertainty in $f_0(1370)$ parameters and its coupling to $\pi^+ \pi^-$ [10], a more definite conclusion is not possible at present.

Acknowledgments

We thank the KEKB group for the excellent operation of the accelerator, the KEK Cryogenics group for the efficient operation of the solenoid, and the KEK computer group and the National Institute of Informatics for valuable computing and Super-SINET network

support. We acknowledge support from the Ministry of Education, Culture, Sports, Science, and Technology of Japan and the Japan Society for the Promotion of Science; the Australian Research Council and the Australian Department of Education, Science and Training; the National Science Foundation of China under contract No. 10175071; the Department of Science and Technology of India; the BK21 program of the Ministry of Education of Korea and the CHEP SRC program of the Korea Science and Engineering Foundation; the Polish State Committee for Scientific Research under contract No. 2P03B 01324; the Ministry of Science and Technology of the Russian Federation; the Ministry of Education, Science and Sport of the Republic of Slovenia; the National Science Council and the Ministry of Education of Taiwan; and the U.S. Department of Energy.

-
- [1] A. Garmash *et al.* (Belle Collaboration), *Phys. Rev.* **D71**, 092003 (2005).
 - [2] K. Abe *et al.* (Belle Collaboration), hep-ex/0509001.
 - [3] B. Aubert *et al.* (BaBar Collaboration), hep-ex/0408032.
 - [4] B. Aubert *et al.* (BaBar Collaboration), hep-ex/0408073.
 - [5] S. Kurokawa, *Nucl. Instr. and Meth.* **A499**, 1 (2003).
 - [6] A. Abashian *et al.*, *Nucl. Instr. and Meth.* **A479**, 117 (2002).
 - [7] Y. Ushiroda (Belle SVD2 Group), *Nucl. Instr. and Meth.* **A511**, 6 (2003).
 - [8] R. Brun *et al.*, GEANT 3.21, CERN Report DD/EE/84-1, 1984.
 - [9] A. Garmash *et al.* (Belle Collaboration), *Phys. Rev.* **D69**, 012001 (2004).
 - [10] S. Eidelman *et al.* (Particle Data Group), *Phys. Lett.* **B592**, 1 (2004).
 - [11] R.H. Dalitz, *Phil. Mag.* **44**, 1068 (1953).
 - [12] M.G. Kendall and A. Stuart, *The Advanced Theory of Statistics*, 2nd ed. (Hafner Publishing, New York, 1968).
 - [13] S.M. Flatté, *Phys. Lett.* **B63**, 224 (1976).
 - [14] P. Chang, *et al.* (Belle Collaboration), *Phys. Lett.* **B599**, 148 (2004).
 - [15] C.S. Kim, B.H. Lim and S. Oh, *Eur. Phys. J.* **C22**, 683 (2002);
C.S. Kim, J.P. Lee and S. Oh, *Phys. Rev.* **D67**, 014002 (2003).